Journal of Materials Chemistry A

# Two-electron-active Tetracyanoethylene for Nonaqueous Redox Flow Batteries



| | |
|---|---|
| Journal: | *Journal of Materials Chemistry A* |
| Manuscript ID | TA-ART-02-2021-001365.R1 |
| Article Type: | Paper |
| Date Submitted by the Author: | 26-Mar-2021 |
| Complete List of Authors: | Wang, Xiao; University of Cincinnati, Chemistry<br>Chai, Jingchao; University of Cincinnati, Chemistry<br>Devi, Nilakshi; University of Cincinnati, Chemistry<br>Lashgari, Amir; University of Cincinnati, Chemistry<br>Chaturvedi, Ashwin; University of Cincinnati, Chemistry<br>Jiang, Jianbing; University of Cincinnati, Chemistry |
| | |

ARTICLE

# Two-electron-active Tetracyanoethylene for Nonaqueous Redox Flow Batteries

Received 00th January 20xx,
Accepted 00th January 20xx

DOI: 10.1039/x0xx00000x

Xiao Wang,[a,†] Jingchao Chai,[a,†] Nilakshi Devi,[a] Amir Lashgari,[a] Ashwin Chaturvedi,[a] Jianbing "Jimmy" Jiang[a,*]

Redox flow batteries (RFBs) are regarded as one of the most promising energy storage devices for efficient utilization of intermittent renewable energy, such as solar and wind energies, yet the development of RFBs has been hindered by the narrow electrochemical window of aqueous electrolytes. Nonaqueous RFB using organic electrolytes is an attractive way to address the abovementioned issue. Here, we report a cyanocarbon-based, two-electron-active anolyte compound, tetracyanoethylene (**TCNE**), with high solubility (2.0 M in acetonitrile), remarkable electrochemical stability and redox reversibility, and fast electrokinetics. Density-functional theory (DFT) calculations for different oxidation states of **TCNE** were performed to evaluate molecular orbitals during the redox processes. Inexpensive and environmentally friendly sodium perchlorate is used as the supporting electrolyte in replacement of the more commonly used and expensive tetraalkylammonium salts. When paired with a phenazine derivative (**PEG1-PTZ**) catholyte, the all-organic nonaqueous RFB exhibits a cell voltage of 1.45 V, a capacity retention of 73.3% over 200 cycles (99.9% per cycle), and a maximum power density of 72.5 mW/cm$^2$. This study introduces a new type of redox-active organic compounds with multi-electron activity, high electrochemical reversibility, and desirable electrokinetics, enriching the family of organic compounds for nonaqueous RFBs.

## Introduction

Increasing energy and environmental concerns have prompted the exploration of renewable energy sources, such as wind, solar, tidal, and geothermal energies.[1-6] In addition to energy capture, the conversion and storage of renewable energy remain one of the most active and challenging research topics.[7-11] Energy storage devices, including supercapacitors, metal ion batteries, metal-air batteries, and redox flow batteries (RFBs), have been successfully applied in various fields because of their unique advantages.[12-17] Compared to the configuration of a conventional battery, where the redox-active materials are confined in the solid-state electrodes, the solution-based redox electrolytes of RFBs are stored in external reservoirs, enabling decoupling of energy and power, as well as superior scalability.[18-21] Both the negative and positive electrolytes, termed as anolyte and catholyte, respectively, circulate through the battery compartments, where the electrochemical reactions occur for energy storage and release.[22-23]

Vanadium-based flow batteries (VRBs), as the most successful commercial RFBs, possess the advantages of excellent safety and long cycling lifetime; however, shortcomings of in-operation VRBs due to the use of highly toxic active materials, highly corrosive acidic electrolytes, and expensive vanadium salts hinder the further development of VRBs.[24-25] Consequently, remarkable attention has been paid to the development of water-soluble, redox-active organic materials due to their structural diversity, low cost, and environmental friendliness.[20,26-29] Even though great progress has been made, the energy density of both VFBs and organic aqueous RFBs has been restricted by the narrow electrochemical window of typical aqueous solutions (< 1.5 V).[30-31]

Nonaqueous organic RFBs (NORFBs) using organic solvents substantially extend the electrochemical window up to 4 V,[32] thus possessing the potential to overcome the drawbacks in aqueous RFBs.[33-35] NORFBs requires high solubility of redox-active organic materials in organic solvents to achieve high energy density. Several organic redox-active materials have been developed for NORFBs, including ferrocene,[36] quinone,[37] phenazine,[38] organometallic complex,[39-40] 2,2,6,6-tetramethylpiperidine-1-oxyl,[41] viologen,[42] and their derivatives. Despite the progress made, the current NORFBs still suffer from the lack of (1) suitable membranes to block the permeation of redox materials to the counter compartment while permitting the transportation of supporting ion for charge balance during charge/discharge,[43] and (2) the redox materials with combined properties of multielectron activity, facile synthesis, high stability, and high solubility.[33,42,44-48] This work is directly relevant to the latter concern, detailing the investigation of a new family of organic materials with the required features for NORFBs.

Cyanocarbons are a group of organic compounds bearing several cyanide units (-C≡N) with special chemical and electrochemical properties.[49] Due to a large number of cyanide groups, cyanocarbons are typically highly conjugated with remarkable redox reversibility.[50]

[a] *Department of Chemistry, University of Cincinnati, P.O. Box 210172, Cincinnati, Ohio 45221-0172, United States.*
† Equal contribution.
*Corresponding author: jianbing.jiang@uc.edu
Electronic Supplementary Information (ESI) available: [details of any supplementary information available should be included here]. See DOI: 10.1039/x0xx00000x

It is also found that the complexation of tetracyanoethylene (**TCNE**) with organometallic compounds results in low reduction potentials.[51] Another counterpart, tetracyanoquinodimethane (**TCNQ**), can be reduced to give a blue-colored radical anion and exhibits excellent redox properties.[52] However, despite a small number of applications of **TCNQ** as organic electrodes in lithium-ion batteries,[53-54] cyanocarbons are rarely used in RFBs.

Here we report the thorough electrochemical investigation of commercially available **TCNE** as a two-electron-active anolyte in NORFBs. The electrochemical properties are studied by a combination of voltammetry, computation, and battery tests. The comparable redox behaviors of **TCNE** in both inorganic (sodium perchlorate, $NaClO_4$) and organic (tetrabutylammonium hexafluorophosphate, $TBAPF_6$) supporting electrolytes suggest that the inexpensive $NaClO_4$ can be used in replacement of the more expensive $TBAPF_6$ in NORFBs. In addition, Density-functional theory (DFT) calculations were performed to evaluate electronic properties and molecular orbitals of different oxidation states of **TCNE** during the redox processes. When paired with the widely used phenothiazine catholyte, the **TCNE**-based battery endows a voltage of 1.49 V with two-electron activity. At a lower **TCNE** concentration of 0.2 M, this battery presents a capacity retention of over 99.9% per cycle and a power density of 72.5 mW/cm$^2$. Higher **TCNE** electrolyte concentration of 0.5 M (= 1.0 M electron concentration) in the **TCNE**-based battery shows negligible capacity fade over 50 cycles, demonstrating great potential of **TCNE** for use in NORFBs.

## Results and discussion

**Physical properties.** The energy density of a RFB is highly dependent on the concentration of the redox-active materials. The solubility of **TCNE** can achieve up to 2.0 M in acetonitrile (MeCN, Figure S1, see the experimental section for testing details), corresponding to a capacity of 107.2 Ah/L based on two-electron activity, which is higher than most of the reported state-of-the-art NORFB materials.[43,55-56] Furthermore, **TCNE** has a superior intrinsic capacity, which is defined as the amount of charge stored in specific mass (per gram) of material.[48,57] With the same number of electrons for half-cell reactions, the smaller the molecular weight, the higher capability of molecules for electron storage.[48] Sanford and co-workers proposed a weight-to-charge ratio of less than 150 g/(mol e$^-$) for anolyte and catholyte materials.[58] The low molecular weight of **TCNE** (128 g/mol) results in an intrinsic equivalent weight of 64 g/(mol e$^-$), which is much smaller than the suggested value, rendering **TCNE** an attractive anolyte candidate.

**Electrochemical properties.** The electrochemical study started with the scrutiny of supporting electrolyte. Tetraalkylammonium hexafluorophosphate or tetrafluoroborate has been widely used as supporting salt in NORFBs, and the more inexpensive and environmentally friendly inorganic salts are rarely reported in NORFBs due to limited solubility and resultant instability of redox-active organic materials.[44] Here, we tested the electrochemical behavior of **TCNE** using both $NaClO_4$ and $TBAPF_6$ in MeCN. The solubility of $NaClO_4$ can reach as high as 2.25 M in MeCN, which is sufficient for application in NORFBs. The study of the redox properties of **TCNE** material starts with CV measurements using 5.0 mM **TCNE** in 0.1 M $NaClO_4$ or $TBAPF_6$ in MeCN. Both $NaClO_4$ and $TBAPF_6$ showed almost identical redox features (Figure S2), thus $NaClO_4$ was used for subsequent electrokinetics and battery studies. Two redox peaks were observed at –0.05 V and –1.08 V vs. Ag/Ag$^+$ (Figure 1A). The widely studied phenazine is selected as the catholyte in this work (Figure 1B). The mixed electrolytes (black trace in Figure 1A) showed the same features as the sum of those from the individual electrolytes (red and blue traces in Figure 1A), suggesting negligible chemical interaction between **TCNE** and **PEG1-PTZ**. We have successfully demonstrated the use of PEGylated phenazine compounds (**PEG12-PTZ** and **PEG3-PTZ**) with 12 and 3 poly(ethylene glycol) (PEG) units, respectively, in our previous studies.[59-61] Here, we further reduced the length of the PEG chain to 1 (thus termed as **PEG1-PTZ**) to decrease the weight-to-charge ratio while still maintaining the high solubility (up to 4.0 M neat concentration). Paired with **PEG1-PTZ** with a redox potential of 0.41 V vs. Ag/Ag$^+$, the **TCNE**-based battery possesses a voltage of 1.49 V.

DFT calculations for **TCNE** for neutral, one-, and two-electron reduced states were performed in order to evaluate orbital energy levels during the redox processes (Figure 1C).[62] The results show that the electron density of the LUMO of **TCNE** and the HOMO of both

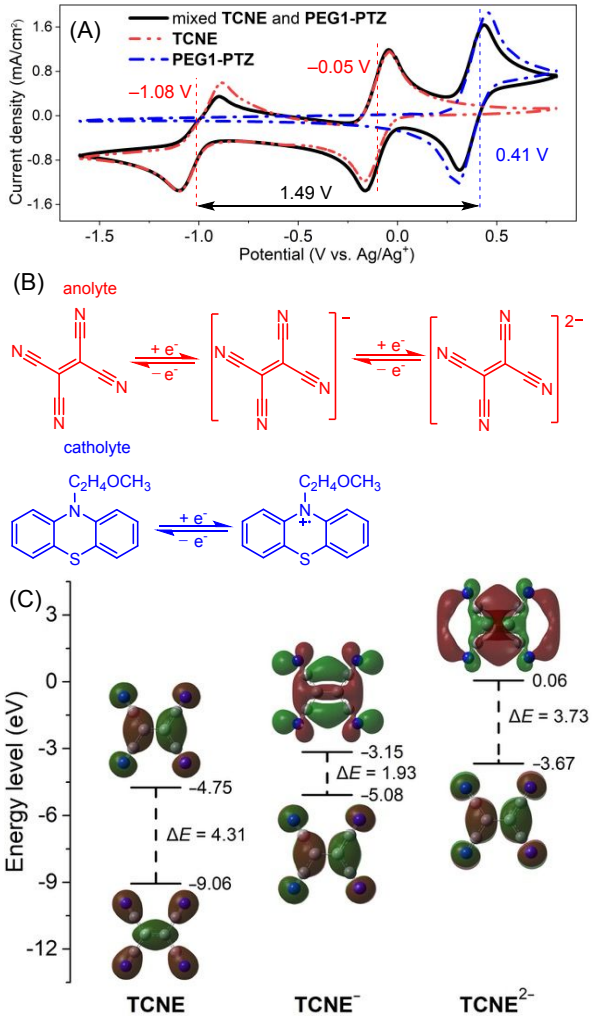


**Figure 1**. (A) Cyclic voltammograms of 5.0 mM **PEG1-PTZ** and **TCNE** on a glassy carbon electrode at the scan rate of 50 mV/s. (B) Redox reactions of **TCNE** and **PEG1-PTZ**. (C) Molecular orbitals (HOMO and LUMO) of neutral and reduced states of **TCNE**.

**TCNE**$^{-}$ and **TCNE2**$^{-}$ orbitals are almost identical and mapped through the compound symmetrically. The calculation result also indicates that the energy band gaps ($\Delta E$) for **TCNE**$^{-}$ is smaller than those of **TCNE** and **TCNE**$^{2-}$. The electron affinity of the first and second reduction events was calculated in the gas phase and MeCN to check the solvent effect. In the gas phase, energy of –3.44 and 1.87 eV was required for first and second electron addition, while these values are –4.90 and –3.39 eV in MeCN. These results show that (1) the binding of the second electron to **TCNE**$^{-}$ is thermodynamically disfavored than the first electron, and (2) the solvent facilitates the second electron binding.[62] Additionally, the electrostatic potential map of the reduced **TCNE** species (Figure S3) represents the electron density maps through the molecule, especially nitrogen atoms, which is responsible for the electron affinity. In addition, the high symmetry of electrostatic potential maps of **TCNE**$^{–}$ and **TCNE**$^{2–}$ indicates that the all four cyano groups of **TCNE** take part in the redox processes.

**Electrokinetics.** The electrokinetics of **TCNE** were studied by CV measurements in the same conditions as above with different scan rates (5–2000 mV/s). A linear trend of current density as a function of the square root of scan rate indicates diffusion-controlled processes on the electrode surface (Figure S4). According to Randles-Sevcik (Equation S1),[63-65] the diffusion coefficients for the first and second reduction events were calculated to be 5.67 x $10^{-6}$ and 9.23 x $10^{-6}$ cm$^2$/s, respectively (see the Experimental section for more detailed calculations). To further characterize the electrochemical kinetics of both reduction events, linear sweep voltammetry (LSV) was performed using 1.0-mM active materials, **TCNE** and **PEG1-PTZ**, in 0.1 M $NaClO_4$/MeCN electrolytes with a rotating disk electrode (RDE).[66] LSV curves of **TCNE** with varied rotation rates are presented in Figure 2A, showing two well-defined plateaus corresponding to the two reduction processes (**TCNE/TCNE**$^{-}$ and **TCNE**$^{-}$**/TCNE**$^{2-}$). Derived from Lévich equation (Equation S2),[67-68] the coefficients for the first and second reduction peaks were determined to be 1.83 x$10^{-6}$ and 4.74 x $10^{-6}$ cm$^2$/s, respectively (Figure 2B). Two different

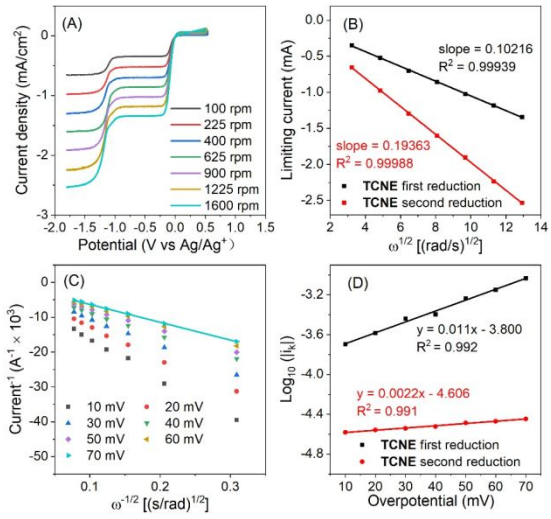


**Figure 2**. (A) Linear sweep voltammetry plots at different rotation rates using a rotating disk electrode. (B) Fitted linear Lévich plots of the limiting current and square root of angular velocity. (C) Koutecký-Levich curve (current$^{-1}$ vs $\omega^{-1/2}$) at different reduction overpotentials of the first reduction of **TCNE**. (D) Tafel plot constructed using the current response and overpotentials. Solution: 1.0 mM **TCNE** in a 0.1 M $NaClO_4$/MeCN solution.

methods gave the same order of magnitude of diffusion coefficients as reported values, [69-70] indicating that the diffusion of **TCNE** on the electrode surface does not limit the redox reaction. Furthermore, the limiting current was obtained from the x-intercept of Tafel plot (Figure 2C, 2D, and Figure S5). According to the Butler–Volmer equation (Equation S3),[18,71] kinetic rate constants of 8.38 x $10^{-3}$ and 1.81 x $10^{-3}$ cm/s were obtained for the first and second reduction processes, respectively (see the Experimental section for more detailed calculations). The catholyte material **PEG1-PTZ** was subjected to the same test, and satisfactory diffusion coefficient (1.75 x $10^{-5}$ cm$^2$/s) and reaction rate constant (8.02 x $10^{-3}$ cm/s) were obtained through similar methods (Figure S6). The high kinetic parameters validate that **TCNE** and **PEG1-PTZ** have satisfactory diffusion properties and electron transfer capabilities in the $NaClO_4$ electrolytes for subsequent battery studies.[72]

**Static battery test.** Since operation lifetime is an important parameter for the application of RFBs, the **TCNE/PEG1-PTZ** static battery was initially tested using mixed electrolytes for both anolyte and catholyte sides to gain insights into the intrinsic property of **TCNE**

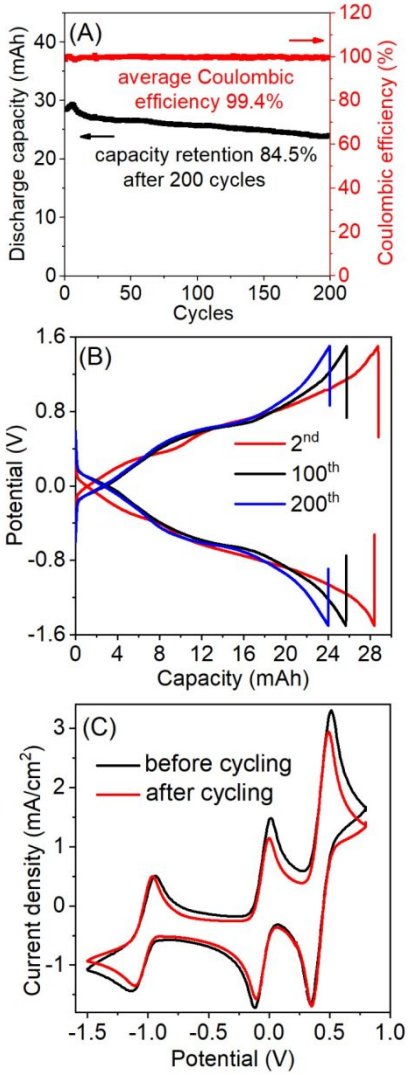


**Figure 3.** (A) Discharge capacity and Coulombic efficiency of the **TCNE** (0.5 M)/**PEG1-PTZ** (1.2 M) static battery at a charge/discharge current density of 20 mA/cm$^2$. (B) Charge/discharge profiles at 2$^{nd}$, 100$^{th}$, and 200$^{th}$ cycles. (C) Cyclic voltammograms of the pre- and post-cycling electrolytes.

using a closed, non-flowing battery setup built in-house (Figure S7). A 0.2 M **TCNE/PEG1-PTZ** static battery was adopted to investigate the long-cycling performance of **TCNE**.[73] After 300 cycles, the battery showed a capacity of 15.1 mAh, retaining 91.5% of the initial capacity (99.97% per cycle) and 70.4% of the theoretical capacity (Figure S8A and S8B). In addition to capacity retention, CV measurement of the pre- and post-cycling electrolytes is also an effective way to evaluate battery stability. As shown in Figure S8C, almost identical CV traces were observed, suggesting high stability and redox reversibility of **TCNE** in the static battery. Furthermore, the negligible change in impedance before and after cycling also indicates the stability of the battery (Figure S8D).

With promising preliminary results for the 0.2 M static battery, we continued with the same measurement at a higher **TCNE** concentration of 0.5 M, corresponding to 1 M electron concentration. The 0.5-M **TCNE/PEG1-PTZ** battery displayed a capacity retention of 84.5% over 200 cycles (from 28.4 to 24.1 mAh), with an average capacity fade rate of 0.078% per cycle (Figure 3A and 3B). Comparable with the 0.2 M static battery, both CV and impedance tests revealed that the increased **TCNE** concentration did not sacrifice the cyclability of the **TCNE** battery (Figures 3C and S9). Even though the static and mixed-electrolyte setup are not suitable for practical applications, the excellent cyclability and low capacity fade rate illustrate the stability of **TCNE** in electrochemical cells, as further demonstrated in the following flow-mode studies.

**RFB test.** The **TCNE/PEG1-PTZ** batteries were also tested in a flow mode at different **TCNE** concentrations. A lower concentration of 0.2 M of **TCNE** was first studied (see the experimental section for details) to explore the battery performance, including charge rate, polarization, energy density, and cyclability. Excess of **PEG1-PTZ** catholyte was used to allow complete electrochemical conversion of **TCNE**. The flow cell presented a discharge capacity of 41.3 mAh, corresponding to 54.6% of the theoretical capacity (Figure 4A and 4B). The battery also exhibited an average capacity retention of 73.3% for 200 cycles (99.9% per cycle) at the current density of 60 mA/cm$^2$ with an average Coulombic efficiency of 99.2% (Figure 4A). The CV of the post-cycling electrolyte showed different features at the second reduction peak (Figure S10), which may be due to the excessive binding force of $Na^+$ and reduced **TCNE** species.[44] Meanwhile, the increased impedance (from 3.4 Ω cm$^2$ to 7.5 Ω cm$^2$) resulted in increase of battery polarization, which is presumably the major cause of capacity degradation. (Figure 4B and 4C).

The rate performance of the battery reflects its electrochemical stability under different charge/discharge conditions. The battery was galvanostatically charged/discharged at current densities from 60 to 100 mA/cm$^2$ (Figure 4D). At a low current density of 60 mA/cm$^2$, the battery delivered a discharge capacity of 37.8 mAh. The discharge capacities at the current densities of 80 and 100 mA/cm$^2$ were 33.6 and 30.7 mAh, respectively (Figure. 4D). Comparison of the area specific resistance (ASR) of the high frequency region, which primarily reflects the resistance of the membrane,[74] to the polarization ASR of the entire battery obtained from LSV at different SOCs shows that the membrane contributes ~70% of the overall resistance (Figures S11 and S12). In addition, the polarization curve of the power density and current density (Figure 4E) exhibits current power density of 72.5 mW/cm$^2$ at 100% SOC, which is comparable with most of the state-of-the-art NORFBs.[72,75]

The 0.5 M **TCNE** flow cell was also successfully demonstrated with a satisfied capacity retention, no obvious capacity fade was observed after 50 cycles (initial capacity 60.2 mAh, 50$^{th}$ cycle capacity

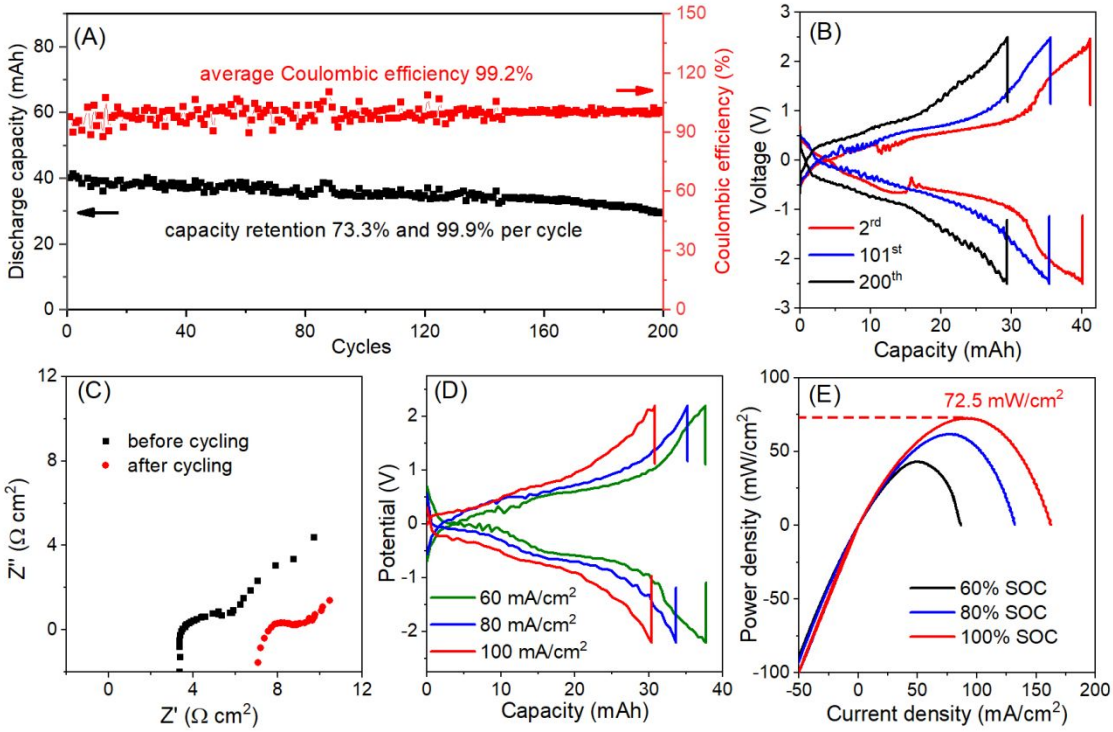


**Figure 4.** Cyclability and rate performance of the **TCNE** (0.2 M)/**PEG1-PTZ** (0.48 M) flow battery. (A) Discharge capacity and Coulombic efficiency over 200 cycles at 60 mA/cm$^2$. (B) Charge/discharge profiles at the 2$^{nd}$, 101$^{st}$, and 200$^{th}$ cycles. (C) Nyquist impedance before and after cycling. (D) Rate performance. (E) Polarizations of the battery at 60%, 80%, and 100% state-of-charge.

ARTICLE

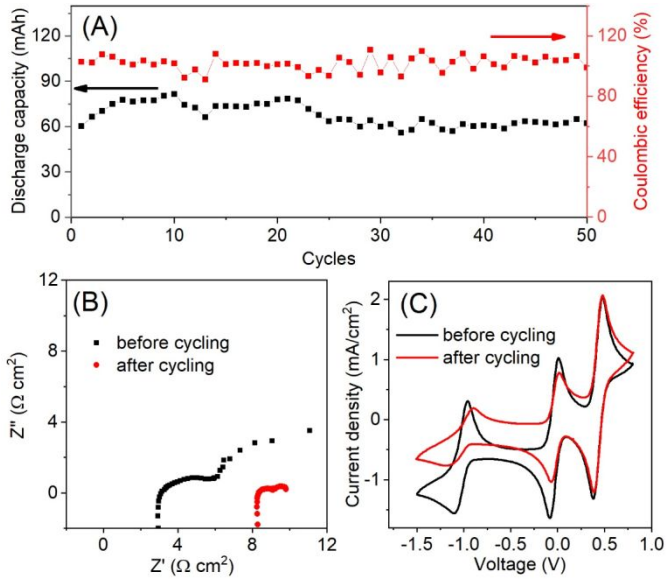


**Figure 5.** The **TCNE** (0.5 M)/**PEG1-PTZ** (1.2 M) flow battery. (A) Discharge capacity and Coulombic efficiency at 60 mA/cm$^2$. (B) Nyquist impedance before and after cycling. (C) Cyclic voltammograms of pre- and post-cycling electrolytes.

62.1 mAh, maximum capacity 84.1 mAh, corresponding to 23.3 Ah/L) (Figure 5). However, the change of electrolyte volume during charging and discharging process due to osmosis and increased electrolyte viscosity also intensified. This leads to greater impedance changes and larger difference in the CV curves before and after cycling (Figure 5B-C). Further improvement of flow cell performance, especially at the high-concentration regime requires insights into the origin of electrolyte viscosity and optimization of the cell design to facilitate mass and charge transfers. Nevertheless, because of the combined features of two-electron activity and high solubility (0.5 M), the theoretical volume energy density of this system can reach as high as 26.6 Wh/L (Equation S4), exceeding most of other flow batteries,[18,72] demonstrating the great potential of **TCNE** as redox-active material for NORFBs.

## Conclusions

We report a new type of two-electron-active organic compound, **TCNE**, as anolyte for NORFB using inexpensive $NaClO_4$ as the supporting electrolyte. The **TCNE/PEG1-PTZ** battery possesses a voltage of 1.49 V and presents excellent capacity retention at different **TCNE** concentrations under both static and flow conditions. Molecular orbital calculations show lower energy gaps and higher electron affinity of reduced **TCNE**. The cell delivers a power density of 72.5 mW/cm$^2$ and shows stable cyclability with an average capacity retention of 99.9% per cycle. Due to the two-electron activity and high solubility of **TCNE**, the 0.5 M **TCNE** battery can exhibit a volumetric energy density of 26 Wh/L. The rapid redox kinetics and high stability render **TCNE** a promising alternative organic compound towards high-performance NORFBs for large-scale energy storage.

## Conflicts of interest

The authors declare no conflict of interest.

## Author Contributions

X. W., J. C., and J. J. conceived and designed experiments. X. W., and J. C. performed battery measurements and analyses. N., D., A., C. and A. L. Synthesized samples. A. L. carried out DFT simulation. All authors discussed the results and revised the manuscript.

## Acknowledgements

The authors acknowledge the University of Cincinnati for startup funding support. NMR experiments were performed on a Bruker AVANCE NEO 400 MHz NMR spectrometer funded by NSF-MRI grant CHE-1726092.

## References

1. Q. Jiang, Y. Zhao, X. Zhang, X. Yang, Y. Chen, Z. Chu, Q. Ye, X. Li, Z. Yin and J. You, *Nature Phys.*, 2019, **13**, 460–466.
2. M. I. Blanco, *Renew. Sust. Energ. Rev.*, 2009, **13**, 1372–1382.
3. G. Egbert and R. Ray, *Nature*, 2000, **405**, 775–778.
4. K. P. Tsagarakis, *Renew. Energ.*, 2020, **147**, 2801–2808.
5. Z. Shao, Z. Wang, Z. Li, Y. Fan, H. Meng, R. Liu, Y. Wang, A. Hagfeldt, G. Cui and S. Pang, *Angew. Chem. Int. Ed.*, 2019, **58**, 5587–5591.
6. H. Wang and H. Dai, *Chem. Soc. Rev.*, 2013, **42**, 3088–3113.
7. M. O. Abdullah, *Applied energy: an introduction*, CRC Press, 2012.
8. N. Panwar, S. Kaushik and S. Kothari, *Renew. Sust. Energ. Rev.*, 2011, **15**, 1513–1524.
9. A. S. Arico, P. Bruce, B. Scrosati, J. M. Tarascon and W. Van Schalkwijk, *Nat. Mater.*, 2005, **4**, 366–377.
10. H. Wang, Y. Yang, Y. Liang, J. T. Robinson, Y. Li, A. Jackson, Y. Cui and H. Dai, *Nano Lett.*, 2011, **11**, 2644–2647.
11. H. Wang, Y. Liang, T. Mirfakhrai, Z. Chen, H. S. Casalongue and H. Dai, *Nano Res.*, 2011, **4**, 729–736.
12. M. Winter and R. J. Brodd, *Chem. Rev.*, 2004, **104**, 4245–4269.
13. Q. Zhou, J. Ma, S. Dong, X. Li and G. Cui, *Adv. Mater.*, 2019, **31**, 1902029.
14. D. Larcher and J. M. Tarascon, *Nat. Chem.*, 2015, **7**, 19–29.
15. J. Sun, H.-W. Lee, M. Pasta, H. Yuan, G. Zheng, Y. Sun, Y. Li and Y. Cui, *Nat. Nanotechnol.*, 2015, **10**, 980.
16. B. Huskinson, M. P. Marshak, C. Suh, S. Er, M. R. Gerhardt, C. J.

Galvin, X. Chen, A. Aspuru-Guzik, R. G. Gordon and M. J. Aziz, *Nature*, 2014, **505**, 195–198.
17. G. Xu, X. Shangguan, S. Dong, X. Zhou and G. Cui, *Angew. Chem. Int. Ed.*, 2020, **59**, 3400–3415.
18. K. Lin, R. Gómez Bombarelli, E. S. Beh, L. Tong, Q. Chen, A. Valle, A. Aspuru-Guzik, M. J. Aziz and R. G. Gordon, *Nat. Energy*, 2016, **1**, 16102.
19. S. O. Tung, S. L. Fisher, N. A. Kotov and L. T. Thompson, *Nat. Commun.*, 2018, **9**, 4193.
20. F. Pan and Q. Wang, *Molecules*, 2015, **20**, 20499–20517.
21. D. G. Kwabi, Y. Ji and M. J. Aziz, *Chem. Rev.*, 2020, **120**, 6467–6489.
22. M. Skyllas-Kazacos, M. H. Chakrabarti, S. A. Hajimolana, F. S. Mjalli and M. Saleem, *J. Electrochem. Soc.*, 2011, **158**, R55.
23. M. Park, J. Ryu, W. Wang and J. Cho, *Nat. Rev. Mater.*, 2016, **2**, 16080.
24. X. Li, H. Zhang, Z. Mai, H. Zhang and I. Vankelecom, *Energy Environ. Sci.*, 2011, **4**, 1147–1160.
25. Y. K. Zeng, T. S. Zhao, L. An, X. L. Zhou and L. Wei, *J. Power Sources*, 2015, **300**, 438–443.
26. A. Z. Weber, M. M. Mench, J. P. Meyers, P. N. Ross, J. T. Gostick and Q. Liu, *J. Appl. Electrochem.*, 2011, **41**, 1137.
27. Y. Zhang, W. Liu, Z. Wang, Y.-M. Shen, W. Wang, Z. Chen, J. Xu and J. Cao, *Carbon*, 2020, **161**, 309–315.
28. Q. Chen, M. R. Gerhardt, L. Hartle and M. J. Aziz, *J. Electrochem. Soc.*, 2016, **163**, A5010–A5013.
29. M. A. Goulet, L. Tong, D. A. Pollack, D. P. Tabor, S. A. Odom, A. Aspuru-Guzik, E. E. Kwan, R. G. Gordon and M. J. Aziz, *J. Am. Chem. Soc.*, 2019, **141**, 8014–8019.
30. W. Wang, W. Xu, L. Cosimbescu, D. Choi, L. Li and Z. Yang, *Chem. Commun.*, 2012, **48**, 6669–6671.
31. B. Hu, J. Luo, M. Hu, B. Yuan and T. L. Liu, *Angew. Chem. Int. Ed.*, 2019, **58**, 16629–16636.
32. J. Zhang, Z. Yang, I. A. Shkrob, R. S. Assary, S. o. Tung, B. Silcox, W. Duan, J. Zhang, C. C. Su, B. Hu, B. Pan, C. Liao, Z. Zhang, W. Wang, L. A. Curtiss, L. T. Thompson, X. Wei and L. Zhang, *Adv. Energy Mater.*, 2017, **7**, 1701272.
33. M. Sanford, A. Shrestha, K. Hendriks, M. Sigman and S. Minteer, *Chem. Eur. J.*, 2020, **26**, 5369–5373.
34. T. Ma, Z. Pan, L. Miao, C. Chen, M. Han, Z. Shang and J. Chen, *Angew. Chem. Int. Ed.*, 2018, **57**, 3158–3162.
35. C. Zhang, Z. Niu, Y. Ding, L. Zhang, Y. Zhou, X. Guo, X. Zhang, Y. Zhao and G. Yu, *Chem*, 2018, **4**, 2814–2825.
36. P. S. Borchers, M. Strumpf, C. Friebe, I. Nischang, M. D. Hager, J. Elbert and U. S. Schubert, *Adv. Energy Mater.*, 2020, **10**, 2001825.
37. Y. Ding, Y. Li and G. Yu, *Chem*, 2016, **1**, 790–801.
38. N. H. Attanayake, J. A. Kowalski, K. V. Greco, M. D. Casselman, J. D. Milshtein, S. J. Chapman, S. R. Parkin, F. R. Brushett and S. A. Odom, *Chem. Mater.*, 2019, **31**, 4353–4363.
39. G. Nagarjuna, J. Hui, K. J. Cheng, T. Lichtenstein, M. Shen, J. S. Moore and J. Rodríguez-López, *J Am. Chem. Soc.*, 2014, **136**, 16309–16316.
40. E. C. Montoto, G. Nagarjuna, J. S. Moore and J. Rodríguez-López, *J. Electrochem. Soc.*, 2017, **164**, A1688–A1694.
41. X. Wei, W. Xu, M. Vijayakumar, L. Cosimbescu, T. Liu, V. Sprenkle and W. Wang, *Adv. Mater.*, 2014, **26**, 7649–7653.
42. B. Hu and T. L. Liu, *J of Energy Chem.*, 2018, **27**, 1326–1332.
43. J. Luo, B. Hu, M. Hu, Y. Zhao and T. L. Liu, *ACS Energy Lett.*, 2019, **4**, 2220–2240.
44. J. Zhang, J. Huang, L. A. Robertson, R. S. Assary, I. A. Shkrob and L. Zhang, *J. Phys. Chem. C*, 2018, **122**, 8116–8127.
45. C. S. Sevov, D. P. Hickey, M. E. Cook, S. G. Robinson, S. Barnett, S. D. Minteer, M. S. Sigman and M. S. Sanford, *J. Am. Chem. Soc.*, 2017, **139**, 2924–2927.
46. J. Zhang, I. A. Shkrob, R. S. Assary, S. o. Tung, B. Silcox, L. A. Curtiss, L. Thompson and L. Zhang, *J. Phys. Chem. C*, 2017, **121**, 23347–23358.
47. X. Wei, W. Xu, J. Huang, L. Zhang, E. Walter, C. Lawrence, M. Vijayakumar, W. A. Henderson, T. Liu, L. Cosimbescu, B. Li, V. Sprenkle and W. Wang, *Angew. Chem. Int. Ed.*, 2015, **54**, 8684–8687.
48. J. Huang, B. Pan, W. Duan, X. Wei, R. S. Assary, L. Su, F. R. Brushett, L. Cheng, C. Liao, M. S. Ferrandon, W. Wang, Z. Zhang, A. K. Burrell, L. A. Curtiss, I. A. Shkrob, J. S. Moore and L. Zhang, *Sci. Rep.*, 2016, **6**, 32102.
49. O. W. Webster, *J Polym. Sci. A Polym. Chem.*, 2002, **40**, 210–221.
50. D. L. Jeanmaire, M. R. Suchanski and R. P. Van Duyne, *J. Am. Chem. Soc.*, 1975, **97**, 1699–1707.
51. T. Roth and W. Kaim, *Inorg. Chem.*, 1992, **31**, 1930–1933.
52. H. Alves, A. S. Molinari, H. Xie and A. F. Morpurgo, *Nat. Mater.*, 2008, **7**, 574–580.
53. Y. Kanzaki, S. Mitani, D. Shiomi, Y. Morita, T. Takui and K. Sato, *ACS Appl. Mater. Interfaces*, 2018, **10**, 43631–43640.
54. Y. Hanyu and I. Honma, *Sci. Rep.*, 2012, **2**, 453.
55. J. Winsberg, T. Hagemann, T. Janoschka, M. D. Hager and U. S. Schubert, *Angew. Chem. Int. Ed.*, 2017, **56**, 686–711.
56. Y. Ding, C. Zhang, L. Zhang, Y. Zhou and G. Yu, *Chem. Soc. Rev.*, 2018, **47**, 69–103.
57. A. Eftekhari, *ACS Sustain. Chem. Eng.*, 2019, **7**, 3684–3687.
58. C. S. Sevov, R. E. Brooner, E. Chenard, R. S. Assary, J. S. Moore, J. Rodríguez-López and M. S. Sanford, *J. Am. Chem. Soc.*, 2015, **137**, 14465–14472.
59. J. Chai, A. Lashgari, Z. Cao, C. K. Williams, X. Wang, J. Dong and J. Jiang, *ACS Appl. Mater. Interfaces*, 2020, **12**, 15262–15270.
60. X. Wang, J. Chai, A. Lashgari and J. Jiang, *ChemElectroChem*, 2020, DOI: 10.1002/celc.202001035, 10.1002/celc.202001035.
61. J. Chai, A. Lashgari, X. Wang, C. K. Williams and J. Jiang, *J. Mater. Chem. A*, 2020, **8**, 15715–15724.
62. R. S. Assary, F. R. Brushett and L. A. Curtiss, *RSC Adv.*, 2014, **4**, 57442–57451.
63. A. Ševčik, *Collect. Czechoslov. Chem. Commun.*, 1948, **13**, 349–377.
64. J. Randles, *Trans. Faraday Soc.*, 1948, **44**, 322–327.
65. J. E. Randles, *Trans. Faraday Soc.*, 1948, **44**, 327–338.
66. H. Wang, S. Y. Sayed, E. J. Luber, B. C. Olsen, S. M. Shirurkar, S. Venkatakrishnan, U. M. Tefashe, A. K. Farquhar, E. S. Smotkin, R. L. McCreery and J. M. Buriak, *ACS Nano*, 2020, **14**, 2575–2584.
67. K. Lin, Q. Chen, M. R. Gerhardt, L. Tong, S. B. Kim, L. Eisenach, A. W. Valle, D. Hardee, R. G. Gordon and M. J. Aziz, *Science*, 2015, **349**, 1529–1532.
68. S. Treimer, A. Tang and D. C. Johnson, *Electroanalysis*, 2002, **14**, 165–171.
69. J. D. Hofmann, S. Schmalisch, S. Schwan, L. Hong, H. A. Wegner, D. Mollenhauer, J. Janek and D. Schröder, *Chem. Mater.*, 2020, **32**, 3427–3438.
70. B. Hu, C. DeBruler, Z. Rhodes and T. L. Liu, *J. Am. Chem. Soc.*, 2017, **139**, 1207–1214.
71. J. Savéant and D. Tessier, *J. Electroanal. Chem. Interf. Electrochem.*, 1975, **65**, 57–66.
72. X. Wei, W. Duan, J. Huang, L. Zhang, B. Li, D. Reed, W. Xu, V. Sprenkle and W. Wang, *ACS Energy Lett.*, 2016, **1**, 705–711.
73. J. D. Milshtein, A. P. Kaur, M. D. Casselman, J. A. Kowalski, S. Modekrutti, P. L. Zhang, N. Harsha Attanayake, C. F. Elliott, S. R. Parkin, C. Risko, F. R. Brushett and S. A. Odom, *Energy Environ. Sci.*, 2016, **9**, 3531–3543.
74. D. G. Kwabi, K. Lin, Y. Ji, E. F. Kerr, M.-A. Goulet, D. De Porcellinis, D. P. Tabor, D. A. Pollack, A. Aspuru-Guzik, R. G. Gordon and M. J. Aziz, *Joule*, 2018, **2**, 1894–1906.
75. W. Duan, J. Huang, J. A. Kowalski, I. A. Shkrob, M. Vijayakumar, E. Walter, B. Pan, Z. Yang, J. D. Milshtein, B. Li, C. Liao, Z. Zhang, W. Wang, J. Liu, J. S. Moore, F. R. Brushett, L. Zhang and X. Wei, *ACS Energy Lett.*, 2017, **2**, 1156c1161.

 